Revista Mexicana de Astronomía y Astrofísica
Universidad Nacional Autónoma de México
rmaa@astroscu.unam.mx
ISSN (Versión impresa): 0185-1101
MÉXICO

2007
A. Königl
MHD DRIVING OF RELATIVISTIC JETS
Revista Mexicana de Astronomía y Astrofísica, marzo, volumen 027
Universidad Nacional Autónoma de México
Distrito Federal, México
pp. 91-101

RevMexAA (Serie de Conferencias), **27**, 91–101 (2007)

MHD DRIVING OF RELATIVISTIC JETS

A. Königl[1]

Received 2005 December 26; accepted 2006 November 3

RESUMEN

Paulatinamente se ha ido reconociendo que los campos magnéticos juegan un papel dominante en la producción y colimación de chorros astrofísicos. Demostramos aquí, usando soluciones semianalíticas exactas para las ecuaciones de MHD ideal en relatividad especial, que un disco de acreción altamente magnetizado (con un campo magnético principalmente poloidal o azimutal) alrededor de un agujero negro es capaz de acelerar un flujo de protones y electrones a los factores de Lorentz y energías cinéticas asociadas a fuentes de destellos de rayos gama y nucleos activos de galaxias. También se discuten las contribuciones a la aceleración provenientes de efectos térmicos (por presión de radiación y pares electrón-positrón) y de MHD no ideal. Notamos que la aceleración por MHD se caracteriza por ser extendida espacialmente, y esta propiedad se manifiesta más claramente en flujos relativistas. Las indicaciones observacionales de que la aceleración de movimientos superlumínicos en chorros de radio ocurre sobre escalas mucho más grandes que las del agujero negro propiamente, apoyan la idea de que la producción de chorros es principalmente un fenómeno magnético. Presentamos resultados preliminares de un modelo global que puede utilizarse para probar esta interpretación.

ABSTRACT

There is a growing recognition that magnetic fields play a dominant role in driving and collimating astrophysical jets. Using exact semianalytic solutions of the special-relativistic ideal-MHD equations, it is demonstrated that a strongly magnetized accretion disk (with a dominant poloidal or azimuthal magnetic field) around a black hole can efficiently accelerate a proton-electron outflow to the Lorentz factors and kinetic energies inferred in gamma-ray burst sources and in active galactic nuclei. The possible contributions of thermal driving (by the pressure of radiation and electron-positron pairs) and of nonideal-MHD effects to the acceleration of the flow are also discussed. It is pointed out that MHD acceleration is distinguished by being spatially extended and that this property should be most noticeable in relativistic flows. It is argued that observational indications that "superluminal" radio jets are accelerated over distances that far exceed the scale of the central black hole support the magnetic-driving picture. Preliminary results of a comprehensive model that could be used to test this interpretation are presented.

Key Words: **GALAXIES: ACTIVE — GALAXIES: JETS — GAMMA RAYS: BURSTS — ISM: JETS AND OUTFLOWS — MAGNETOHYDRODYNAMICS**

1. INTRODUCTION

The acceleration and collimation of jets in a variety of astronomical objects are often attributed to the action of magnetic fields (e.g., Livio 2000; Königl & Pudritz 2000). It is commonly envisioned that magnetic field lines threading a rotating compact object or its surrounding accretion disk can efficiently tap the rotational energy of the source and accelerate gas to high speeds through centrifugal and/or magnetic pressure-gradient forces. It is argued that the hoop stresses of the twisted field lines can account for the narrowness of many jets and that, at least in some cases, alternative production mechanisms (such as thermal driving) can be excluded on observational grounds.

Until fairly recently, much of the theoretical work on jets concentrated on the nonrelativistic regime. This has been motivated by the fact that most of the outflows that were studied observationally (primarily large-scale extragalactic radio jets and jets from young stellar objects) were inferred to move at nonrelativistic speeds, and that even in the case of the blazar class of active galactic nuclei (AGNs), where relativistic bulk flows were indicated by apparent superluminal motions and rapid Stokes-parameter variability, the implied (terminal) bulk Lorentz factors γ_∞ were typically not much greater than 1. This situation has now changed on account of the follow-

[1]Dept. of Astronomy & Astrophysics, U. Chicago, IL, USA.

ing developments: (1) In the case of AGNs, apparent superluminal speeds that imply values of γ_∞ as high as $\sim 40\,c$ have been recorded (e.g., Jorstad et al. 2001). (2) Observations of long-duration gamma-ray bursts (GRBs) and their afterglows have been convincingly interpreted in terms of ultrarelativistic ($\gamma_\infty \sim 10^2 - 10^3$) jets (e.g., Piran 1999). (3) Apparent superluminal motions of radio features with implied values of γ_∞ that can exceed ~ 10 have been measured also in Galactic black-hole and neutron-star binaries (e.g., Fender et al. 2004). These findings have highlighted the strong similarities among the various types of relativistic jet sources and have focused attention on the question of their origin. Although the physical scales of the outflows can be very different— AGN jets are inferred to emanate from the vicinity of a supermassive ($\sim 10^8 - 10^{10}\,M_\odot$) black hole, whereas long-duration GRB outflows are evidently associated with a newly formed stellar-mass black hole or rapidly rotating neutron star—it is believed that magnetic driving is still the underlying driving mechanism in all of these cases (e.g., Blandford 2002b). The current challenge for theorists is to devise quantitative models for the relativistic regime that can be tested by the new observations.

Recent developments in the modeling of relativistic magnetohydrodynamic (MHD) outflows are presented in § 2 of this contribution. Applications to GRB and AGN sources are discussed in §§ 3 and 4, respectively. The conclusions and a brief outline of work in progress are given in § 5.

2. EXACT RELATIVISTIC-MHD SOLUTIONS

This section describes the derivation of exact relativistic-MHD jet solutions representing initially Poynting-dominated configurations that convert a large fraction of their electromagnetic energy into relativistic bulk motion of baryons. For definiteness, it is assumed that the jet originates in a disk around a central compact object (e.g., a stellar-mass black hole in the case of a GRB source or a supermassive black hole in an AGN). It is further assumed that the disk is threaded by a large-scale, well-ordered magnetic field, although flow acceleration and collimation could conceivably be produced even if the field were small-scale and tangled (e.g., Heinz & Begelman 2000; Li 2002). Instead of tapping the rotational kinetic energy of the disk, the outflow might harness the rotational energy of the central object—through the stellar magnetic field in the case of a neutron star (e.g., Usov 1994; Kluźniak & Ruderman 1998) or a field supported by the disk in the case of a black hole (e.g., Blandford & Znajek 1977; van Putten & Levinson 2003)—but this should not affect the qualitative nature of the outflow at large distances from the origin. The quantitative details could, however, change from source to source as they depend on the boundary conditions (magnetic flux distribution, angular velocity distribution, and mass loading) at the origin. The basic properties of the outflow are modeled on the assumption that it can be properly described by the equations of special-relativistic, ideal MHD. While the exact behavior of the flow in the immediate vicinity of the compact objects requires a fully general-relativistic treatment, it is shown below that the bulk of the jet acceleration generally occurs on scales where these effects can be neglected. The application of the ideal MHD equations to the problem of highly relativistic outflows has been questioned by Blandford (2002a; see also Lyutikov & Blandford 2002), who adopted instead a force-free electromagnetic description (which has the benefit of being computationally more tractable); it is, however, worth noting that a force-free behavior can be recovered from the relativistic MHD formulation as a limiting case of negligible particle mass and pressure. Although finite-conductivity effects (associated with magnetic reconnection) might play a role in the jets (see § 5), the formal validity conditions for ideal MHD are typically well satisfied for the solutions presented here (e.g., Vlahakis & Königl 2001).

The initial (subscript i) field amplitude at the base of the flow that is required for driving the outflow can be inferred from an estimate of the injected energy. For example, in the case of GRBs, $\mathcal{E}_i$ = (Poynting flux) × (surface area) × (burst duration). For a jet element with an initial cylindrical radius ϖ_i and radial width $(\Delta\varpi)_i$, $\mathcal{E}_i \approx cE_iB_{\phi,i}\varpi_i(\Delta\varpi)_i\Delta t$, where the electric field is given by $E = B_{\rm p}V_\phi/c - B_\phi V_{\rm p}/c$ (with the subscripts p and ϕ denoting the poloidal and azimuthal components, respectively). For characteristic parameters of long-duration GRBs ($\mathcal{E}_i \approx 10^{52}$ ergs, $\varpi_i \sim (\Delta\varpi)_i \approx 10^6$ cm, $\Delta t \approx 10$ s), one infers $B_i \sim 10^{14} - 10^{15}$ G. This field is most plausibly generated by differential-rotation amplification of a much weaker poloidal field component that was originally present in the disk (see discussion in Vlahakis & Königl 2003b). If $|B_{\rm p,i}/B_{\phi,{\rm i}}| > 1$, a *trans-Alfvénic* outflow is produced, whereas if $|B_{\phi,{\rm i}}/B_{\rm p,i}| > 1$, the outflow is *super-Alfvénic* from the start. The latter situation may correspond to amplified toroidal flux loops that have been disconnected by magnetic reconnection and escape from the disk surface in a nonsteady fashion.

The system of equations of special-relativistic, ideal MHD consists of the Maxwell and Euler equations together with the mass and specific-entropy conservation relations. Assuming axisymmetry [$\partial/\partial\phi = 0$ in spherical $(r\,,\theta\,,\phi)$ and cylindrical $(\varpi\,,\phi\,,z)$ coordinates] and a steady state, the full set of equations can be partially integrated to yield several field-line constants (e.g., Lovelace et al. 1986). The assumption of a steady state is applicable if the magnetic flux distribution at the source is approximately constant on the time scale of interest and, in the case of distinct ejections as in GRBs, if the Lorentz factor of the poloidal motion of the ejected shell satisfies $\gamma_{\rm p} \gg 1$ (Vlahakis & Königl 2003a). The field-line constants are the total specific angular momentum $L(A)$, the field angular velocity $\Omega(A)$, the "magnetization parameter" $\sigma_{\rm M}(A)$ (with the mass-to-magnetic flux ratio given by $A\Omega^2/\sigma_{\rm M}c^3$), the adiabat $Q(A) \equiv P/\rho_0^{\Gamma}$ (with the index Γ being either 4/3 or 5/3, corresponding to relativistic and nonrelativistic temperatures, respectively), and the total energy-to-mass flux ratio $\mu(A)c^2 = \xi\gamma c^2 + (c/4\pi)(E|B_\phi|/\gamma\rho_0 V_{\rm p})$. Here $A = (1/2\pi)\int\int \mathbf{B}_{\rm p}\cdot d\mathbf{S}$ is the poloidal magnetic flux function (which identifies the field line), $\mathbf{V}$ is the bulk velocity, γ is the Lorentz factor, ρ_0 and P are the comoving matter density and pressure, and $\xi c^2 = c^2 + 5P/2\rho_0$ is the specific enthalpy. The variable ξ makes it possible to incorporate thermal effects into the model. Although purely hydrodynamic driving of relativistic jets can probably be ruled out (see, e.g., Di Mateo et al. 2002 and Daigne & Mochkovitch 2002 for the GRB case, and Vlahakis & Königl 2004 for AGNs), thermal forces may nonetheless dominate the initial acceleration of magnetic outflows (e.g., Mészáros, Laguna, & Rees 1993; see § 3). An initial value $\xi_i \gg 1$ could correspond to a "hot" electron-positron/radiation component that dominates the thermal pressure.

Vlahakis & Königl (2003a,b; hereafter VK) obtained exact solutions of the above equations by integrating the two remaining relations (the Bernoulli and transfield force-balance equations) under the assumption of radial self-similarity of the form $r = \mathcal{F}_1(A)\mathcal{F}_2(\theta)$ (see Figure 1). With this ansatz it is possible to separate the $(A\,,\theta)$ variables if the following relations hold (cf. Vlahakis & Tsinganos 1998): $\mathcal{F}_1(A) \propto A^{1/F}$, $L(A) \propto A^{1/F}$, $\Omega(A) \propto A^{-1/F}$, $Q(A) \propto A^{-2(F-2)/3}$, $\mu(A) = const$, and $\sigma_{\rm M}(A) = const$ (see Li, Chiueh, & Begelman 1992 and Contopoulos 1994 for the "cold" limit of this model). The parameter F controls the distribution of the poloidal current I: $2|I|/c = \varpi|B_\phi| = A^{1-1/F}\mathcal{F}(\theta)$.

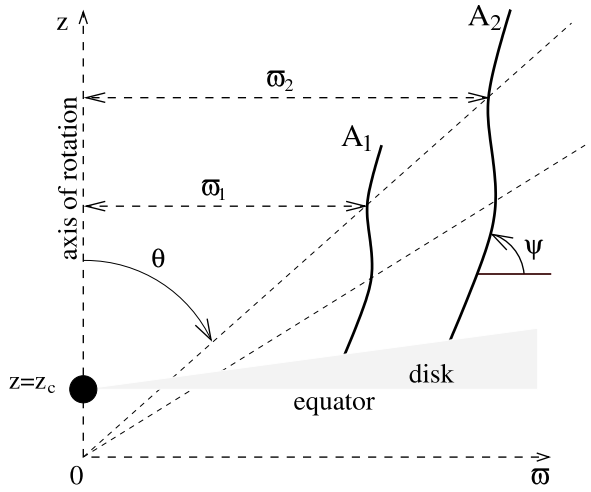

Fig. 1. Sketch of r self-similar field lines in the meridional plane. For any two field lines A_1 and A_2, the ratio of cylindrical distances for points corresponding to a given value of θ is the same for all the cones $\theta = const$.

Close to the origin the field is force-free: $\mathcal{F}(\theta) \approx const$, and hence $\varpi|B_\phi| \propto A^{1-1/F}$. Thus, the parameter regime $F > 1$ corresponds to a current-carrying jet, with the poloidal current density being antiparallel to the magnetic field ($J_\parallel < 0$; see Figure 2). In this case the current tends to zero as the symmetry axis is approached, so such solutions should provide a good representation of the conditions near the axis of a highly collimated flow. Conversely, solutions with $F < 1$ correspond to the return-current regime (in which the poloidal current density is parallel to the field, $J_\parallel > 0$) and are most suitable at larger cylindrical distances. Although the detailed global current distribution cannot be modeled using the self-similarity approach, one can nevertheless generate "hybrid" flow configurations that combine a current-carrying solution for low values of ϖ and a return-current solution for high values of ϖ (see Figure 4). Initially Poynting-dominated flows that attain a rough equipartition between the kinetic and Poynting energy fluxes at large distances from the origin have F close to 1. When $F > 1$ the Lorentz force can collimate the flow to cylindrical asymptotics. For $F < 1$ the collimation is weaker and the flow only reaches conical asymptotics; however, the acceleration is more efficient in this case in that a larger fraction of the Poynting flux is converted into kinetic energy.

The original radially self-similar MHD jet model constructed by Blandford & Payne (1982) in the nonrelativistic regime corresponds to $F = 0.75$. Thus, in

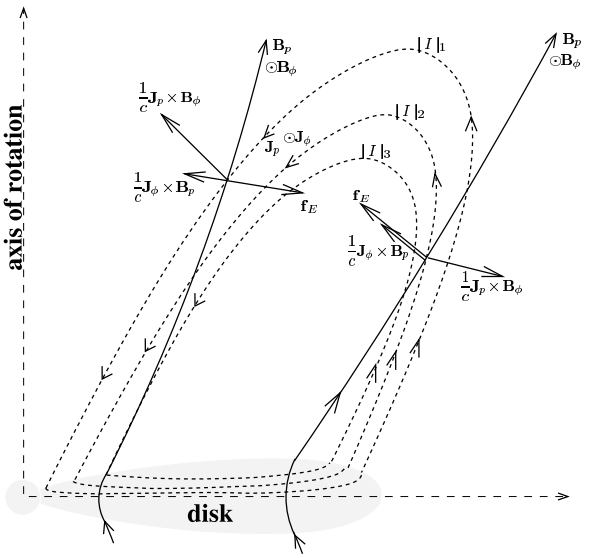

Fig. 2. Sketch of two meridional field lines (solid) and three meridional current lines (dashed). The meridional current lines represent the loci of constant total poloidal current ($I = const$). The magnetic and electric forces are shown for the current-carrying ($J_\parallel < 0$, *l*eft field line) and return-current ($J_\parallel > 0$, *r*ight field line) cases.

contrast with the relativistic solutions derived by VK (which have $F > 1$ near the origin), it has a singularity in I at $\varpi = 0$, a feature for which it has sometimes been critiqued (although note that the vicinity of the axis can typically be excluded in practical disk applications). A basic difference between the relativistic and nonrelativistic self-similar models is the existence of a characteristic speed, c, in the relativistic case, which precludes the incorporation of gravity into the self-similar equations and a simple matching of the outflow solution to a particular (e.g., Keplerian) disk rotation law, as was done in the Blandford & Payne (1982) solution. [VK were able to mitigate this limitation by allowing the height z_c of the disk to vary (see Figure 1); for $z_c = 0$, $\Omega \propto 1/\varpi$ along the conical surface of the disk, whereas for $z_c > 0$ the decrease of Ω with ϖ is steeper.] The relativistic-MHD regime is further complicated by the fact that the displacement current and the charge density cannot be neglected in the formulation.

The variable separation transforms the original P.D.E.'s into O.D.E.'s, and one seeks a solution by integrating these equations. The general problem requires the specification of seven constraints: four associated with the boundary conditions at the source and three determined by the regularity requirements at the critical points of the joint solution of the Bernoulli and transfield equations. Representative solutions that illustrate the general properties of magnetically driven relativistic jets are presented in the next two sections.

3. APPLICATION TO GRB OUTFLOWS

This section is divided into two parts. First, a generic solution that demonstrates the ability of the magnetic driving model to account for the inferred basic properties of GRB outflows is presented and analyzed. In the second part, the "baryon loading" problem for disk-driven GRB jets is addressed in the context of an initially neutron-rich MHD outflow model, and additional observational implications of this picture are outlined.

3.1. *Poynting Flux-Dominated MHD Jet Solutions*

Long-duration ($\gtrsim 2$ s) GRBs have been inferred to arise in ultrarelativistic, highly collimated (opening half-angle $\theta_{\rm j} \sim 2^\circ - 20^\circ$) outflows of typical kinetic energy $E_{\rm K} \sim 10^{51}$ ergs. Early models of GRB outflows have interpreted them in terms of thermally driven "fireballs" powered by neutrino emission or magnetic field dissipation at the source. However, the current view is that magnetic fields provide the most plausible means of extracting the inferred energy on the burst time scale (e.g., Mészáros & Rees 1997; Di Mateo et al. 2002). VK verified that magnetic fields can also guide, collimate, and accelerate the flow. In particular, their derived semianalytic solutions demonstrate that Poynting flux-dominated disk outflows (either trans- or super-Alfvénic) can transform $\gtrsim 50\%$ of their magnetic energy into kinetic energy of $\gamma_\infty \sim 10^2 - 10^3$ baryons.

A representative solution is shown in Figure 3. It describes a trans-Alfvénic flow in the current-carrying regime. The outflow is "hot" ($\xi_i \gg 1$) and corresponds to a "fast rotator" ($\mu \gg \xi_i$). Initially, the acceleration is predominantly thermal and the magnetic field only guides and collimates the flow. The behavior of the flow in this regime is completely analogous to that of a classical fireball, except that the spherical radius r in the scaling relations is replaced by the cylindrical radius ϖ (see Vlahakis & Königl 2001). The thermal acceleration zone terminates when ξ decreases to ~ 1, at which point $\gamma \approx \xi_i$. The bulk of the acceleration, however, takes place on larger scales in the magnetic acceleration region, where the Poynting energy (represented by the top curve in Figure 3*a*) is converted into kinetic energy (represented by the γ curve). The acceleration by the Lorentz force corresponds to the decrease of $|\varpi B_\phi|$ along the poloidal streamlines. The

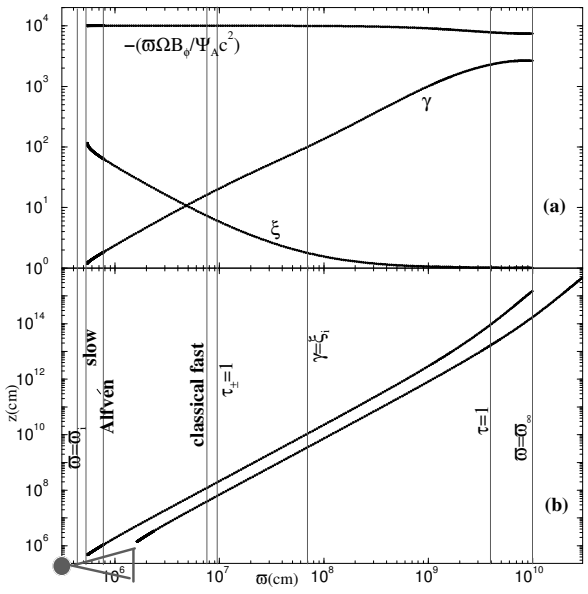

Fig. 3. Illustrative relativistic-MHD solution of a GRB outflow. (*a*) Poynting (top) and enthalpy (ξ) energy fluxes, normalized by the mass flux $\times\, c^2$, and the Lorentz factor (γ) as functions of height along a fiducial magnetic field line. (*b*) Meridional projections of the innermost and outermost field lines are shown on a logarithmic scale, along with a sketch of the black-hole/debris-disk system. The vertical lines mark the positions of various relevant transition points along the innermost field line.

large value of γ_∞ attained by the flow can be attributed to the large extent of the acceleration region. In fact, the acceleration continues all the way to the *modified* fast-magnetosonic surface (the "event horizon" for the propagation of fast-magnetosonic waves), which is situated well beyond the classical fast-magnetosonic surface (Figure 3*b*). The acceleration terminates when the flow collimates to a cylinder (after which time ϖB_ϕ no longer varies along the streamlines).

An extended region over which the magnetic "spring" uncoils and drives the flow is characteristic of MHD acceleration models and distinguishes them from purely hydrodynamic scenarios. This mechanism operates also in nonrelativistic MHD flows (Vlahakis et al. 2000), but the effect should be easier to discern in relativistic jets. The relatively high efficiency of Poynting-to-kinetic energy conversion that can be attained in this model makes it possible to attribute at least some of the γ-ray emission in GRBs to colliding shells (the "internal shock" scenario; e.g., Piran 1999). On the other hand, the fact that a significant fraction of the Poynting energy may remain untapped makes it in principle possible to utilize the magnetic energy directly in the emission process (e.g., Spruit, Daigne, & Drenkhahn 2001) and might also have implications to the subsequent afterglow emission (e.g., the relative weakness of the emission from the reverse shock driven into the decelerating ejecta).

3.2. *Neutron-Rich MHD Jets*

If one compares the estimated mass of protons in a typical long-duration GRB jet [$M_{\rm proton} = 3 \times 10^{-6}(E_{\rm K}/10^{51}\ {\rm ergs})(\gamma_\infty/200)^{-1}\ M_\odot$] with the minimum mass of the debris disk from which the jet could plausibly originate (obtained under the assumption that at most $\sim 10\%$ of the disk gravitational potential energy is converted into outflow kinetic energy), one finds that the outflow can comprise at most $\sim 10^{-4}$ of the disk mass. However, disk outflow models that utilize a large fraction of the disk potential energy typically also entail substantial mass loading—this is the essence of the GRB "baryon loading" problem. One approach to this issue has been to postulate that the outflow emerges along magnetic field lines that thread the black-hole event horizon and not the disk, but then the converse problem — how to avoid having too few baryons — must be addressed (e.g., Levinson & Eichler 2003). A possible resolution of the problem in the context of disk-fed jet models was proposed by Fuller, Pruet, & Abazajian (2000), who noted that such outflows are expected to be neutron-rich [the initial neutron/proton ratios could be as high as $({\rm n/p})_i \sim 20 - 30$]. Since only the charged outflow component couples to the electromagnetic field, the neutrons could potentially decouple from the protons before the latter attain their terminal Lorentz factor. In this picture, the inferred value of $M_{\rm proton}$ may represent only a small fraction of the total baryonic mass ejected from the disk, which would alleviate the loading problem. However, it can be shown that, for purely hydrodynamic outflows, the Lorentz factor $\gamma_{\rm d}$ at decoupling is at least a few times 10^2. This implies that $\gamma_{\rm d}/\gamma_\infty \sim 1$ and hence that the protons end up with only a small fraction of the injected energy, which is *not* a satisfactory resolution of the problem.

Vlahakis, Peng, & Königl (2003) argued that the incorporation of magnetic fields makes it in principle possible to attain $\gamma_{\rm d} \ll \gamma_\infty$ and thereby reclaim the promise of the Fuller et al. proposal. They modeled the pre-decoupling region using a "hot" super-Alfvénic outflow solution. A general property of such solutions is that, during the initial thermal acceler-

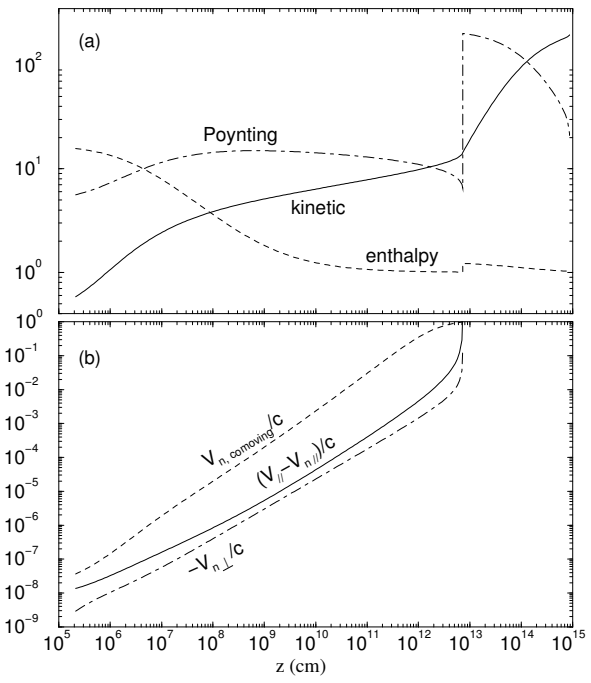

Fig. 4. Illustrative relativistic-MHD solution of a neutron-rich outflow. (*a*) Components of the total energy flux, normalized by the mass flux $\times\, c^2$, as functions of height along a fiducial magnetic field line. The Poynting and enthalpy curves are discontinuous at the decoupling point, reflecting the decrease in the mass flux of field-coupled gas above that point. (*b*) Components of the proton–neutron drift velocity.

ation phase, a fraction of the enthalpy flux is converted into Poynting flux . This reduces the acceleration rate, so at the point of decoupling (when $V_{\rm proton} - V_{\rm neutron} \sim c$) the Lorentz factor is still comparatively low. The energy deposited into the Poynting flux is returned to the matter beyond the decoupling point as kinetic energy, thereby enhancing the acceleration efficiency of the proton component. The end result is a large $\gamma_\infty/\gamma_{\rm d}$ ratio *and* comparable terminal kinetic energies in the proton and neutron components, in clear contradistinction to the purely hydrodynamic solutions.

An illustrative solution [with $({\rm n/p})_i = 30$] is shown in Figure 4. This is a "hybrid" configuration (see § 2) in that the pre-decoupling and post-decoupling regions correspond to the current-carrying ($F = 1.05$) and return-current ($F = 0.1$) regimes, respectively. In this case the enthalpy flux initially dominates the Poynting flux("slow rotator" regime, $\xi_i \approx \mu$), but the charged component nevertheless collimates from an initial opening half-angle of 55° to $\theta_{\rm j} \approx 7°$. The thermal acceleration effectively terminates at a height $z \approx 10^9$ cm above the disk, and the neutrons decouple from the protons at $z_{\rm d} \approx 10^{13}$ cm with $\gamma_{\rm d} \approx 15$. By the time of decoupling the neutrons have acquired $\sim 2/3$ of the injected energy, with the remainder residing predominantly in the electromagnetic field. The latter portion is then transferred with almost 100% efficiency into proton kinetic energy, so that, ultimately, the protons have $\gamma_\infty = 200$ and $E_{\rm K,proton} \approx 10^{51}$ ergs $\approx 0.5\, E_{\rm K,neutron}$. The proton jet thus carries $\sim 1/3$ of the injected energy but only $\sim 3\%$ of the injected mass. Figure 4*b* shows that, even though the decoupling in this case is initiated by the growth of the n–p drift velocity along the poloidal magnetic field, there is also a transverse drift component (induced by the ongoing magnetic collimation), which at the time of decoupling is $|V_{\rm neutron\perp}| \sim 0.1\, c$.

The decoupled neutrons undergo β decay into protons at a distance $\sim 4 \times 10^{14}\, (\gamma_{\rm d}/15)$ cm. In contrast with the situation in purely hydrodynamic outflow models (Pruet & Dalal 2002; Beloborodov 2003), there may well be *no* interaction between the two decoupled components in the MHD case since their motions are not collinear. The latter scenario thus gives rise to a 2-component outflow: an outer (wider) component (comprising the decoupled neutrons) that carries most of the energy and may be responsible (after the neutrons decay) for the bulk of the optical/radio afterglow, and an inner (narrower) component (comprising the original protons) that accounts for the prompt γ-rays and possibly also for some of the X-ray afterglow. A 2-component outflow of this type was inferred in GRB 030329 (Berger et al. 2003; Sheth et al. 2003). General implications of such a model to the afterglow lightcurves and to the energetics of GRB and X-ray flash sources were considered by Peng, Königl, & Granot (2005; see Figure 5). A 2-component jet interpretation could potentially also help to account for some of the apparent peculiarities of the early afterglow emission that were revealed by recent *Swift* observations (Granot, Königl, & Piran 2006).

4. APPLICATION TO BLAZAR JETS

The MHD acceleration model also provides a natural interpretation of "superluminal" AGN jets. In contrast with GRB outflows (or jets from Galactic X-ray binaries, for that matter), the acceleration zone in blazars is evidently resolvable by radio interferometry. This makes relativistic AGN jets prime candidates for testing and constraining this model. The evidence for parsec-scale acceleration in blazars and an illustrative model fit are presented in the first

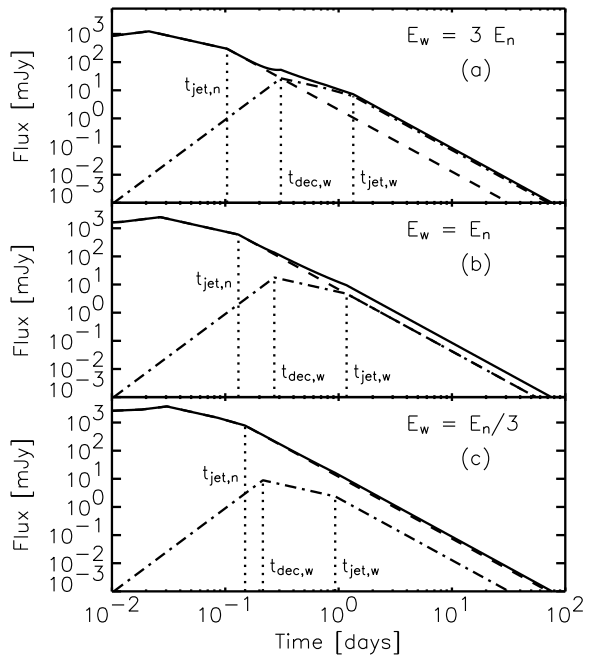

Fig. 5. R-band afterglow lightcurves for a two-component jet with representative parameters. Results are given for different ratios of the kinetic energies of the two components, with the total outflow energy fixed at 10^{51} ergs. The contribution of the narrow component ($\theta_{\rm j,n} = 0.05$), wide component ($\theta_{\rm j,w} = 0.15$), and their sum is shown by the dashed, dash-dotted, and solid curves, respectively. The nominal deceleration and jet-break times for the two components are also indicated.

part of this section. Further observational tests are considered in § 4.2.

4.1. *Parsec-Scale Accelerations*

A growing body of data indicates that relativistic AGN jets undergo the bulk of their acceleration on parsec (more generally, $\sim 0.1 - 10$ pc) scales. In particular, the absence of bulk-Comptonization spectral signatures in blazars has been argued to imply that Lorentz factors $\gtrsim 10$ must be attained on scales $\gtrsim 10^{17}$ cm (Sikora et al. 2005). In the case of the quasar 3C 345, Unwin et al. (1997) combined a VLBI proper-motion measurement of the jet component C7 with an inference of the Doppler factor from an X-ray emission measurement (interpreted as SSC radiation) to deduce an acceleration from $\gamma \sim 5$ to $\gamma \gtrsim 10$ over $r \sim 3-20$ pc. Piner et al. (2003) inferred an acceleration from $\gamma = 8$ at $r < 5.8$ pc to $\gamma = 13$ at $r \approx 17.4$ pc in the quasar 3C 279 jet using a similar approach. Extended acceleration in the 3C 345 jet has been independently indicated by the increase in apparent component speed with separation from the nucleus (Lobanov & Roland 2005) and by the observed luminosity variations of the moving components (Lobanov & Zensus 1999). Similar effects in other blazars (e.g., Homan et al. 2001a) suggest that parsec-scale acceleration may be a common feature of AGN jets.

The inferred large-scale accelerations in AGN jets are very hard to interpret naturally in purely hydrodynamic terms since in the latter class of models the acceleration generally saturates on the much smaller scale of the central mass distribution, which sets the size of the sonic "nozzle." Extended acceleration is, however, a signature of MHD driving, as discussed in § 3.1, and one can reproduce the observed behavior using the semianalytic model described in § 2 (Vlahakis & Königl 2004). Figure 6 shows an illustrative fit to the 3C 345 data presented by Unwin et al. (1997). It is worth bearing in mind, however, that the kinematic data used in obtaining this fit do not uniquely determine the solution: exactly the same flow speeds and field-line shape are obtained if the density, particle pressure, and squared amplitudes of the magnetic field components are rescaled by the same factor.

Panels (*c*)–(*g*) in Figure 6 show various quantities as functions of $\varpi/\varpi_{\rm A}$ (which, in turn, is a function of the polar angle θ) along the outermost field line. (Here $\varpi_{\rm A}$ is the Alfvén lever arm, and $\varpi_{\rm A,out} = 150\,\varpi_{\rm A,in} = 4.1\times10^{-2}$ pc in this example.) Panel (*c*) depicts the force densities in the poloidal direction, showing that thermal and centrifugal effects are important only near the origin, with the magnetic pressure-gradient force rapidly becoming the dominant driving mechanism. Panel (*d*), in turn, shows that, asymptotically, an approximate equipartition between the kinetic and Poynting fluxes is attained ($\gamma_\infty \approx \mu/2$). This panel also demonstrates that the model fit reproduces well the inferred acceleration of component C7. For the adopted fiducial parameters, this component is predicted to continue accelerating up to $\gamma_\infty \approx 35$. Interestingly, Lorentz factors of this order have been inferred in the more distant components (in particular C3 and C5) of the 3C 345 jet (Lobanov & Zensus 1999).

Panels (*e*) and (*f*) depict the bulk velocity components and the temperature, respectively. Even if the initial temperature is as high as $\sim 10^{12}$ K, thermal effects are overall insignificant—this is thus an effectively "cold" ($\xi_i \approx 1$) outflow. Panel (*g*) shows that the magnetic field is primarily poloidal near the origin of the flow but becomes predominantly azimuthal further downstream. Asymptotically, $B_z \propto \varpi^{-2}$, $-B_\phi \propto \varpi^{-1}$, and also $B_\varpi << B_z$—a signature

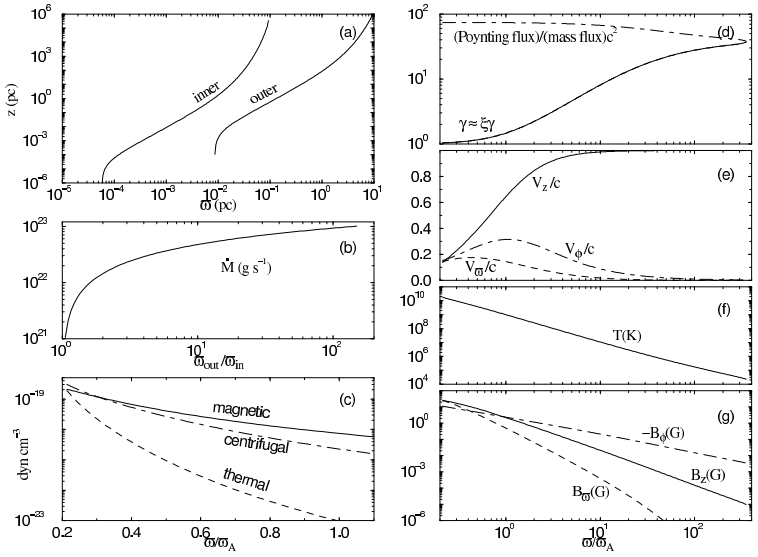

Fig. 6. r self-similar solution describing the superluminal jet in 3C 345. (a) Poloidal field-line shape on a logarithmic scale. (b) Mass-loss rate as a function of $\varpi_{\rm out}/\varpi_{\rm in}$, the ratio of the outermost and innermost disk radii. The remaining panels are discussed in the text.

of cylindrical collimation. As in the case of the GRB outflow solutions presented in § 3, the results presented in Figure 6 demonstrate that MHD driving implies that jet collimation (and not just acceleration) takes place over an extended region (although the rate of field-line bending is reduced with increasing Lorentz factor as the effective inertia goes up and the electric force becomes nearly as large as — and almost cancels out — the transverse magentic force). This predicted behavior is also supported by observations of relativistic jets (e.g., Junor, Biretta, & Livio 1999). It is conceivable that a slower wind from the outer regions of the accretion disk that feeds the central source could aid in the collimation of the relativistic outflow that emanates from the innermost region (e.g., Bogovalov & Tsinganos 2005).

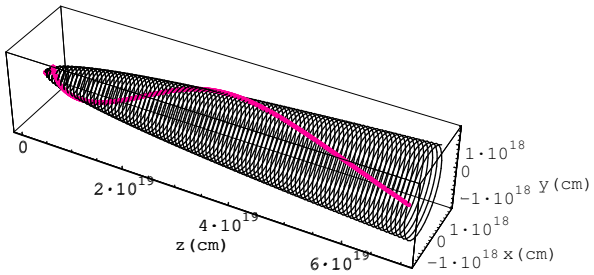

Fig. 7. Visualization of the 3C 345 jet model of Figure 6, showing the shape of magnetic field lines anchored near the fiducial outermost disk radius (*thin line*) and an isolated fluid streamline emerging from that radius (*thick line*).

4.2. *Comprehensive Modeling of Parsec-Scale Jets*

The VLBI-traced paths of superluminal components in blazar jets are typically curved and are often well approximated by helical trajectories (see, e.g., Steffen et al. 1995 for the case of 3C 345). A magnetically driven jet from a circumnuclear accretion disk could exhibit a helical flow pattern if it were ejected from a localized region (in both r and ϕ) on the disk surface. Physically, this would correspond to mass loading of only an isolated flux bundle that threads the disk (see Camenzind & Krockenberger 1992). Figure 7 shows a realization of this possibility corresponding to the 3C 345 model fit presented in Figure 6. In particular, this figure depicts the shape of a streamline that originates near the outer boundary of the model disk (along which the motion closely reproduces the acceleration data for component C7). Also shown is the shape of the magnetic field line on the surface of an axisymmetric outflow from the same disk radius—the difference between these two curves can be understood from the fact that, whereas the poloidal velocity is parallel to the poloidal field under ideal-MHD conditions, the matter angular velocity is close to that of the field line only near the base of the flow and becomes much smaller further out. Figure 8 demonstrates that the

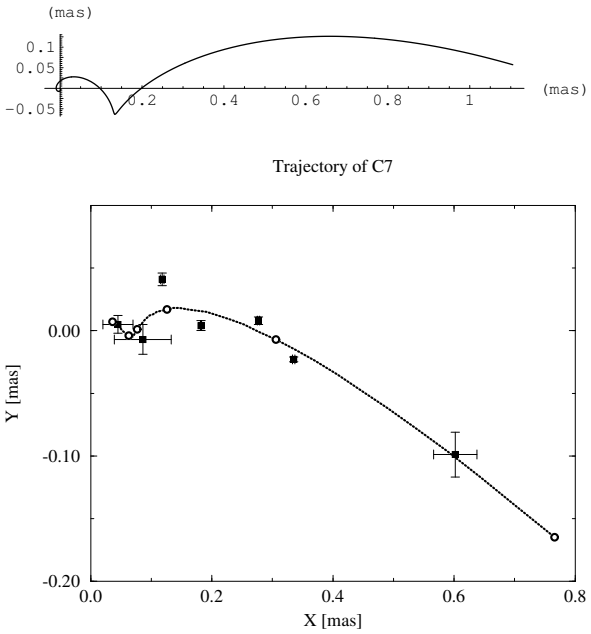

Fig. 8. **Top:** projection of the streamline shown in Figure 7 on the plane of the sky, with the x axis corresponding to the projected jet axis. **Bottom:** data points for component C7 in the 3C 345 jet (from Lobanov 1996).

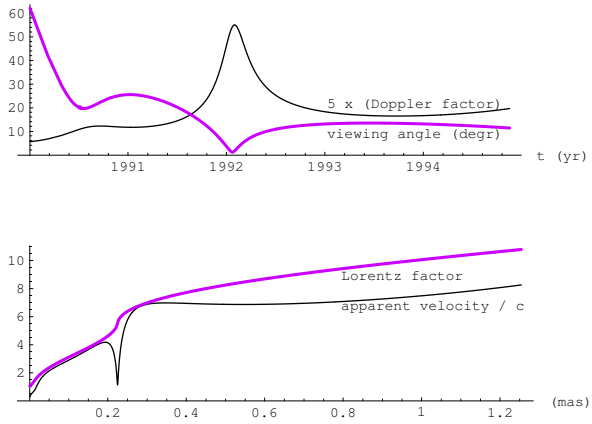

Fig. 9. Preliminary fits to the evolution of component C7 in 3C 345, using the magnetic outflow model shown in Figure 6. **Top:** (*a*) Doppler factor and viewing angle (*thin* and *thick* curves, resp.) as functions of time in the observer's frame. **Bottom:** (*b*) Apparent speed and Lorentz factor (*thin* and *thick* curves, resp.) as functions of distance along the projected jet axis.

model fit to the projected trajectory on the plane of the sky is in good agreement with the observations.

The incorporation of observational input on the jet's kinematic properties could help constrain the model parameters and might be useful in distinguishing a "minimal" model, wherein magnetic field effects account for the observed acceleration as well as for the helical trajectories, from alternative interpretations in which the jet's shape is due to other effects (such as current-driven or Kelvin-Helmholtz instabilities—e.g., Hardee 2000, or gravitationally induced precession at the source—e.g., Scheuer 1992; Kaastra & Roos 1992; Katz 1997). In fitting the motion of a distinct jet component along an isolated streamline, one needs to specify the initial disk radius r_0 and azimuthal angle ϕ_0 at the disk surface as well as the angle $\theta_{\rm obs}$ between the line of sight and the jet axis. One can attempt to obtain approximate values for these parameters by trying to optimize the fit to the time evolution of the apparent speed and Doppler factor [from which the evolution of γ and θ can be derived by using $\beta_{\rm app} = \beta \sin\theta/(1-\beta\cos\theta)$ and $\mathcal{D}^{-1} = \gamma(1-\beta\cos\theta)$] together with the fit to the shape of the projected trajectory.

Figure 9*a* depicts a tentative realization of this procedure for component C7 in 3C 345, which has yielded $r_0 \approx 2\times10^{16}$ cm, $\phi_0 \approx 180°$, and $\theta_{\rm obs} \approx 9°$.

Figure 9*b* demonstrates that a superluminal component moving along a helical trajectory may exhibit an apparent deceleration during an early phase of its evolution even as its Lorentz factor continues to increase. This behavior has been observed in knot C7 of 3C 345 (e.g., Zensus 1997) as well as in other superluminal jet components.

5. SUMMARY AND FUTURE PROSPECTS

The main results discussed in this contribution can be summarized as follows:

- Magnetic fields likely play a prominent role in the extraction of rotational energy at the source as well as in the guiding, acceleration, and collimation of relativistic outflows from compact astronomical objects (GRB sources, AGNs, and Galactic black-hole and neutron-star binaries).
- Exact semianalytic solutions of special-relativistic ideal MHD can account for GRB and AGN jets.
- An extended acceleration region is a distinguishing characteristic of MHD driving of relativistic outflows. In the case of AGN jets the acceleration zone can probably be resolved by radio interferometry, which may make it possible to test and constrain this model.

It would be desirable to complement the semianalytic approach that has been used to establish the ba-

sic properties of relativistic MHD outflows with numerical work. By suitably modifying the self-similar solutions to apply to a finite grid, one could employ the semianalytic results for initiating and testing numerical calculations. The envisioned simulations could, in turn, be used to test the generality and stability of the semianalytic solutions; they should also be useful in exploring new parameter-space regimes and the behavior of nonsteady outflows. There are already several existing relativistic-MHD numerical codes that could potentially be applied to this problem, and some of them even incorporate general relativity and can be used to model the details of the outflow launching process (e.g., McKinney & Gammie 2004; De Villiers et al. 2005; Komissarov 2005). It is worth noting, however, that no existing numerical calculation spans the range in scales that is required for explicitly demonstrating the acceleration to a high Lorentz factor; in fact, the high terminal Lorentz factors inferred in some of these simulations (e.g., McKinney 2006) only represent estimates of the maximum achievable (rather than determinations of the actually attained) values (see also Komissarov 2005). In this respect, the self-similar solutions are currently still the best indicators of the global behavior of relativistic MHD outflows. Inasmuch as these solutions do not incorporate gravity, they do not accurately model the launching process, although this deficiency could be mitigated by employing non–self-similar semianalytic solutions for the base of the jet (e.g., Levinson 2006) to locate the slow-magnetosonic surface of the outflow.

Even under the assumption that ideal MHD is a good approximation for treating the dynamics of relativistic jets, departures from this state could conceivably lead to a direct conversion of magnetic energy into nonthermal radiation. This possibility had been considered in the context of pulsar-type scenarios for GRBs (e.g., Usov 1994; Thompson 1994) and was also discussed in connection with AGN jets (e.g., Choudhuri & Königl 1986; Romanova & Lovelace 1997.) The dissipation of magnetic energy naturally results in a decrease in the azimuthal magnetic field component along the outflow, and the magnetic pressure gradient established in this fashion could contribute to the flow acceleration (Drenkhahn & Spruit 2002). The incorporation of this effect into a semianalytic jet-acceleration model is currently under study.

The potential importance of a two-component GRB jet of the type that arises naturally in the initially neutron-rich MHD outflow model (§ 3.2) provides a motivation for further studies of this scenario. The original dynamical treatment of the neutron-rich outflow (Vlahakis et al. 2003) was based on the single-fluid equations. A more general treatment, which considers the neutrons and the charged-particle component separately, would give a more accurate representation of the neutron decoupling process. Further insight into this process could be gained by combining the dynamical model with detailed thermal-structure and nuclear-reactions calculations.

To fully capitalize on the potential of superluminal jet sources for testing the basic magnetic acceleration model, one can supplement the kinematic constraints considered in § 4.2 with constraints provided by the radiative properties of the outflow. Since the dominant emission process in these jets is evidently synchrotron radiation, which is intimately tied to the intrinsic magnetic field structure, one could in principle gain valuable insights from a comparison of the emitted flux density, the linear and circular polarizations, and the Faraday rotation measure with the model predictions. Work on these generalizations has already begun. The results of linear-polarization and Faraday-rotation measurements in relativistic parsec-scale AGN jets are consistent with the presence of a pervasive helical magnetic-field configuration in these sources (e.g., Gabuzda 2003; Gabuzda, Murray, & Cronin 2004; Lyutikov, Pariev, & Gabuzda 2005). Circular polarization has also been detected in many blazars, and there is a clear indication that these sources exhibit a preferred handedness (or sign) that may persist for decades (e.g., Homan, Attridge, & Wardle 2001b). Perhaps the most natural interpretation of this finding is that it reflects the twist imprinted on the ordered magnetic field in the jet by the rotation of the source (e.g., Ensslin 2003). Given that model fits to helical component trajectories in a superluminal jet can in principle yield an independent determination of the sense of rotation of the source (see Figs. 7–9), a measurement of the sign of circular polarization in such a jet might provide a check on the underlying kinematic model.

I am grateful to Nektarios Vlahakis, Fang Peng, and Jonathan Granot for their contributions to the work reported in this article. This research was supported in part by NASA Astrophysics Theory Program grant NAG5-12635.

REFERENCES

Beloborodov, A. M. 2003, ApJ, 585, L19
Berger, E., et al. 2003, Nature, 426, 154

Blandford, R. 2002a, in Lighthouses of the Universe, ed. M. Gilfanov et al. (Berlin: Springer), 38
Blandford, R. D. 2002b, Lect. Notes Phys., 589, 227
Blandford, R. D., & Payne, D. G. 1982, MNRAS, 199, 883
Blandford, R. D., & Znajek, R. L. 1977, MNRAS, 179, 433
Bogovalov, S., & Tsinganos, K. 2005, MNRAS, 357, 918
Camenzind, M., & Krockenberger, M. 1992, A&A, 255, 59
Choudhuri, A. R., & Königl, A. 1986, ApJ, 310, 96
Contopoulos, J. 1994, ApJ, 432, 508
Daigne, F., & Mochkovitch, R. 2002, MNRAS, 336, 1271
De Villiers, J.-P., Hawley, J. F., Krolik, J. H., & Hirose, S. 2005, ApJ, 620, 878
Di Matteo, T., Perna, R., & Narayan, R. 2002, ApJ, 579, 706
Drenkhahn, G., & Spruit, H. C. 2002, A&A, 391, 1141
Ensslin, T. A. 2003, A&A, 401, 499
Fender, R., Wu, K., Johnston, H., Tzioumis, T., Jonker, P., Spencer, R., & van der Klis, M. 2004, Nature, 427, 222
Fuller, G. M., Pruet, J., & Abazajian, K. 2000, Phys. Rev. Lett., 85, 267
Gabuzda, D. C. 2003, NewARev, 47, 599
Gabuzda, D. C., Murray, E., & Cronin, P. 2004, MNRAS, 351, L89
Granot, J., Königl, A., & Piran, T. 2006, MNRAS, 370, 1946
Hardee, P. E. 2000, ApJ, 533, 176
Heinz, S., & Begelman, M. C. 2000, ApJ, 535, 104
Homan, D. C., Attridge, J. M., & Wardle, J. F. C. 2001b, ApJ, 556, 113
Homan, D. C., Ojha, R., Wardle, J. F. C., Roberts, D. H., Aller, M. F., Aller, H. D., & Hughes, P. A. 2001a, ApJ, 549, 840
Jorstad, S. G., Marscher, A. P., Mattox, J. R., Wehrle, A. E., Bloom, S. D., & Yurchenko, A. V. 2001, ApJS, 134, 181
Junor, W., Biretta, J. A., & Livio, M. 1999, Nature, 401, 891
Kaastra, J. S., & Roos, N. 1992, A&A, 254, 96
Katz, J. I. 1997, ApJ, 478, 527
Kluźniak, W., & Ruderman, M. 1998, ApJ, 505, L113
Königl, A., & Pudritz, R. E. 2000, in Protostars and Planets IV, ed. V. Mannings, A. P. Boss, & S. S. Russell (Tucson: Univ. Arizona Press), 759
Komissarov, S. S. 2005, MNRAS, 359, 801
Levinson, A. 2006, ApJ, 648, 510
Levinson, A., & Eichler, D. 2003, ApJ, 594, L19
Li, L.-X. 2002, ApJ, 564, 108
Li, Z.-Y., Chiueh, T., & Begelman, M. C. 1992, ApJ, 394, 459
Livio, M. 2000, in AIP Conf. 522, Cosmic Explosions, ed. S. S. Holt, & W. W. Zhang (Melville: AIP), 275
Lobanov, A. P. 1996, PhD Thesis, New Mexico Inst. Mining Tech.
Lobanov, A. P., & Roland, J. 2005, A&A, 431, 831
Lobanov, A. P., & Zensus J. A. 1999, ApJ, 521, 509
Lovelace, R. V. E., Mehanian, C., Mobarry, C. M., & Sulkanen, M. E. 1986, ApJS, 62, 1
Lyutikov, M., & Blandford, R. D. 2002, in Beaming and Jets in Gamma Ray Bursts, ed. R. Ouyed (eConf C0208122), 146
Lyutikov, M., Pariev, V. I., & Gabuzda, D. C. 2005, MNRAS, 360, 869
McKinney, J. C. 2006, MNRAS, 368, 1561
McKinney, J. C., & Gammie, C. F. 2004, ApJ, 611, 977
Mészáros, P., Laguna, P., & Rees, M. J. 1993, ApJ, 415, 181
Mészáros, P., & Rees, M. J. 1997, ApJ, 482, L29
Peng, F., Königl, A., & Granot, J. 2005, ApJ, 626, 966
Piner, B. G., Unwin, S. C., Wehrle, A. E., Zook, A. C., Urry, C. M., & Gilmore, D. M. 2003, ApJ, 588, 716
Piran, T. 1999, Phys. Rep., 314, 575
Pruet, J., & Dalal, N. 2002, ApJ, 573, 770
Romanova, M. M., & Lovelace, R. V. E. 1997, ApJ, 475, 97
Scheuer, P. A. G. 1992, in Extragalactic Radio Sources - From Beams to Jets, ed. J. Roland, H. Sol, & G. Pelletier (Cambridge: Cambridge Univ. Press), 368
Sheth, K., et al. 2003, ApJ, 595, L33
Sikora, M, Begelman, M. C., Madejski, G. M., & Lasota, J.-P. 2005, ApJ, 625, 72
Spruit, H. C., Daigne, F., & Drenkhahn, G. 2001, A&A, 369, 694
Steffen, W., Zensus, J. A., Krichbaum, T. P., Witzel, A., & Qian, S. J. 1995, A&A, 302, 335
Thompson, C. 1994, MNRAS, 270, 480
Unwin, S. C., Wehrle, A. E., Lobanov, A. P., Zensus J. A., Madejski, G. M., Aller, M. F., & Aller, H. D. 1997, ApJ, 480, 596
Usov, V. V. 1994, MNRAS, 267, 1035
van Putten, M. H. P. M., & Levinson, A. 2003, ApJ, 584, 937
Vlahakis, N., & Königl, A. 2001, ApJ, 563, L129
_____. 2003a, ApJ, 596, 1080 (VK)
_____. 2003b, ApJ, 596, 1104 (VK)
_____. 2004, ApJ, 605, 656
Vlahakis, N., Peng, F., & Königl, A. 2003, ApJ, 594, L23
Vlahakis, N., & Tsinganos, K. 1998, MNRAS, 298, 777
Vlahakis, N., Tsinganos, K., Sauty, C., & Trussoni, E. 2000, MNRAS, 318, 417
Zensus, J. A. 1997, ARA&A, 35, 607

Arieh Königl: Department of Astronomy & Astrophysics, University of Chicago, 5640 S. Ellis Ave., Chicago, IL 60637, USA (arieh@jets.uchicago.edu).